MODELING CONFINED FLUIDS WITH THE MULTICOMPONENT POTENTIAL THEORY OF ADSORPTION AND THE SAFT-VR MIE EQUATION OF STATE

A Thesis

by

AHMED MOHAMED AHMED ALYAZIDI

Submitted to the Office of Graduate and Professional Studies of
Texas A&M University
in partial fulfillment of the requirements for the degree of

MASTER OF SCIENCE

Chair of Committee,	Ioannis G. Economou
Co-Chair of Committee,	Marcelo Castier
Committee Member,	Thomas Seers
Head of Department,	Arul Jayaraman

August 2020

Major Subject: Chemical Engineering

ABSTRACT

In this work, the SAFT-VR Mie equation of state is combined with the Multi-component Potential Theory of Adsorption (MPTA) in order to describe the phase-equilibrium behavior of confined fluids due to their presence in an external field, namely a solid-fluid potential field. This is important for the understanding, modeling and design of fluids confined in micro- and meso-pores pertinent to applications in hydrocarbon reservoirs, membrane-based separations and heterogeneous catalytic systems, to name but a few. The problem specifications are the temperature of the system, volume of the pores, and the number of moles of each component in the system. The formulation results in the minimization of the Helmholtz energy of the system subject to mass and pore-volume conservation constraints. This formulation, in addition to treating supercritical fluids, tackles the problem of pore-condensation of subcritical systems by employing a Helmholtz-based global phase stability analysis which allows us to detect the presence of phase instability inside the pores as well as locate the spatial location at which it takes place.

ACKNOWLEDGEMENTS

CONTRIBUTORS AND FUNDING SOURCES

NOMENCLATURE

Roman Letters

a – Dimensionless form of the Helmholtz energy

a^M – Helmholtz energy of the reference monomer

a^{HS} – Helmholtz energy of the reference hard sphere

a_1, a_2, a_3 – Expansion terms of the reference monomer Helmholtz energy

A – Helmholtz energy

A_{jm}^{in} – Internal Helmholtz energy of component i in layer j of region m

A_{jm}^{f} – Field Helmholtz energy of component i in layer j of region m

A_{jm} – Helmholtz energy in layer j of region m

g_{ii}^{Mie} – Radial distribution function (RDF) of Mie fluids for component i

H_m – Total pore width in region m

$H_{in,m}$ – Internal pore width in region m (excluding the adsorbent radius, σ_s)

k – The Boltzmann constant

l_m – Number of layers in region m

m_i – Number of monomeric segments per chain molecule

n_{ijm} – Number of moles of component i in layer j of region m

nc – Number of components

N_m^{ads} – Number of moles adsorbed in region m

n_i – Total number of moles of component i

N_s – Number of monomeric segments

P – Bulk phase pressure

r – Number of regions

r_{conf} – Number of confined regions

s_i – Number of associating sites on component i

T – System temperature

V – Total volume of the system

V_m – Total volume of a region

v – Molar volume

v_{jm} – Molar volume of layer j in region m

X_{a_i} – Fraction of component i not bonded on site a

$x_{B,i}$ – Mole fraction of component i in the bulk phase

x_{im}^{ads} – Concentration of component i adsorbed in region m

x_{im}^{ex} – Excess concentration of component i adsorbed in region m

z_{jm} – Distance from the center of the pore to the confining wall

Greek Letters

α – Empirical parameter in the Steele potential

β – $\frac{1}{kT}$

$\hat{\beta}$ – Solid heterogeneity parameter

Γ – Surface excess

Δ_{abij} – Association strength between site a on component i and site b on component j

Δ_m – Interlayer spacing of the adsorbent

δ – Kronecker delta function

$\varepsilon_{s,im}$ – Solid-fluid energy interaction parameter

ε_{0i} – Characteristic energy of component i

θ^*_{ijm} – Local composition

μ_{ijm} – Chemical potential of component i in layer j in region m

ρ_B – Molar density of the bulk phase

ρ_{sm} – Density of the solid (adsorbent) in region m

σ_{ii} – Molecular diameter of component i

$\sigma_{s,im}$ – Solid-fluid diameter

a, b – Associating site

i, k – Component

j – Layer

m – Region

f – Field contribution

int – Internal field contribution

TABLE OF CONTENTS

LIST OF FIGURES

LIST OF TABLES

1. INTRODUCTION

Confinement within porous media has a substantial effect on the thermophysical properties and phase behavior of fluids. Accounting for the effect of confinement explicitly requires a modification in the fundamental thermodynamic equations in order to account for interactions between the fluid molecules and the confining solid. Generally, state functions such as entropy, enthalpy and Helmholtz energy are chosen to be minimized according to the type of problem: adiabatic expansion, reversible compression, and storage tank, respectively. Taking the case of a constant-volume storage tank as an example, the specifications are the temperature, volume of the tank and component amounts (T,V,N) resulting in the minimization of the Helmholtz energy of the system, as formulated based on a chosen equation of state which accounts for intermolecular interactions between fluid molecules. This minimization is performed constrained by the conservation of the number of moles of each component.

In systems which experience external fields, such as that of a solid-fluid potential or gravity, the use of a standard equation of state on its own is no longer sufficient because it only takes into account the interactions among fluid molecules. Conventionally, different approaches are employed to tackle this problem from Monte Carlo (MC) and Molecular Dynamics (MD) simulations to density functional theory (DFT) calculations. Molecular simulation studies provide a lot of insight into the interactions between the confined fluid molecules and pore walls but they generally entail a large number of calculations which are too computationally cumbersome and time-consuming to be used in engineering applications in chemical process calculations. Density functional theory calculations, although less computationally demanding than molecular simulations, are still rarely used in process design calculations. This

is possibly due to their complexity.

The use of equations of state, modified for confined fluids, is an approach which is of intermediate complexity and uses less computational power and time than molecular simulations and DFT calculations. Therefore, such an approach can be utilized in standard chemical process design calculations. In this approach, the effect of confinement is incorporated into the formulation of the Helmholtz energy under some simplifying assumptions. One of the important simplifying assumptions is that the fluid-solid potential depends solely on the distance from the solid wall, neglecting the effect of the two-dimensional layers of adsorbed fluid on the fluid-fluid interactions near the wall. This assumption results in two independent contributions to the Helmholtz energy: one from the equation of state, which depends solely on the temperature, volume and number of moles, and one from the solid-fluid potential which only depends on the perpendicular distance between the fluid molecule and the solid wall. Such a formulation ensures that at a distance, far from the wall, the confinement contribution vanishes leaving behind the contribution of the equation of state only. The confinement contribution limiting case can also be reached when the solid-fluid energy of interaction is set to zero, such as the case of non-attractive pore walls.

An additional feature brought upon by using an equation of state is the prediction of capillary condensation and the determination of its location in the pore. Such capability is achieved by using a Helmholtz-based Global Phase Stability Test (A-GPhST). In A-GPhST calculations, the objective function being minimized is the difference between the Helmholtz energy of the original system and that of a two-phase system (the original system with a trial phase). The objective function is thus minimized. If the system is found to be unstable, indicating the occurrence of capillary condensation, initial estimates are generated to be used in the addition of

2

a new phase. After phase addition,the Helmholtz energy minimization is repeated for the entire system. [1].

The aim of this project is to extend and enhance a previously developed model [2] which combined the Multicomponent Potential Theory of Adsorption (MPTA) with cubic equations of state to account for a larger class of chemical species and wider range of conditions. This new extended model combines the MPTA framework with the SAFT-VR Mie equation of state and a Helmholtz-based global phase stability test in order to accurately predict the properties of associating as well as non-associating fluids and predict the occurrence of pore condensation at subcritical conditions. In order for this aim to be realized, the following list of objectives needed to be achieved:

1. Implement the SAFT-VR Mie equation of state, including its association term, and validate it by reproducing vapor-liquid equilibrium data reported in the literature for the same EoS.

2. Integrate the SAFT-VR Mie EoS with the adsorption model and validate it by reproducing adsorption isotherms and local density profiles reported for the same adsorption model but with a cubic EoS. The goal of this is to validate the basic function of the model.

3. Implement a Helmholtz-based global phase stability test (A-GPhST) based on the SAFT-VR Mie EoS and validate it by reproducing coexistence curves for multiple systems reported in the literature for the same A-GPhST model based on the Peng-Robinson EoS.

4. Optimize solid-fluid energy parameters for the MPTA-SAFT-VR Mie model and validate such parameters by reproducing experimental adsorption isotherms reported in the literature.

1.1 Outline and Scope of this Work

The outline of this thesis is as follows: Section 2 presents a literature review of various theoretical models and computational approaches used to study the effect of confinement on a plethora of adsorbent-adsorbate systems covering a variety of research fields and applications. This is important to place this work in a proper context.

Section 3 lays out the theoretical background for the different models employed by highlighting the model's most important equations and the sources from which they were obtained. This section also describes the algorithm followed in solving the model equations with commentary on some important numerical details and the software used.

Section 4 outlines the results of this work, discusses the findings and compares the performance of the model with similar models cited from the literature.

Finally, some conclusions from the results are drawn in Section 5. A bibliography of the works cited can be found in the References list and large tabulated results were placed in Appendix A.

2. LITERATURE REVIEW OF ADSORPTION MODELS

Throughout the 20th century, many models and theories have been developed to predict the behavior of fluids confined by pores. In this section, some noteworthy theoretical and computational developments in the study of adsorption are briefly discussed.

2.1   Langmuir Theory

Langmuir's theory is one of the earliest attempts to model the adsorption of fluids on solid surfaces. In its early formulation, it was assumed that the solid adsorbent surface consists of a lattice of adsorption sites onto which the adsorbate molecules attach during the process of adsorption. Such sites have equivalent energies associated with the chemical species that make up the surface. Two other major assumptions of the Langmuir theory are that fluid adsorbate molecules that reside in adjacent sites do not interact with one another and that they only form one molecular layer of the adsorbed phase in what is known as 'unimolecular adsorption' [3]. This formulation was used to model the adsorption of a perfect gas on flat, energetically homogeneous adsorbent surfaces [4]. The Langmuir model, although too simple to yield good agreement with a wide range of experimental data, has been an important starting point for many adsorption models that came after [5]. In later years, Fowler and Guggenheim extended the statistical mechanical formulation of the Langmuir theory to account for 'lateral interactions' between adjacently-adsorbed fluid molecules and hence improved the Langmuir model's capability to predict phase change at the gas-solid interface [5]. Other scientists, such as Sips and Tóth, modified the Langmuir theory to improve on some of its shortcomings such as the assumption of energetic homogeneity of the adsorbent surface [6, 7].

Perhaps one of the most noteworthy developments was brought upon by Brunauer, Emmet and Teller [8] who extended the formulation of Langmuir to encompass 'multilayer adsorption'. The result of their work is the famous BET isotherm [5]. In their model, it was assumed that adsorbate molecules can form multiple layers on top of the adsorbent surface and the Langmuir equation is applied to each layer of the adsorbate fluid. The energy of adsorption used for those layers are equivalent to the condensation energy of the fluid [8]. The most important application of the BET adsorption isotherm has been as a means to quantify the surface area of porous solids from adsorption data.

2.2   Potential Theory Models

Polanyi [9], in his work of 1914, first formulated the Potential Theory of Adsorption by proposing a view of adsorption analogous to other potential fields such as the gravitational potential field. According to this view, the adsorbent surface generates a potential field of which the strength is inversely proportional to the distance from the adsorbent surface. This relationship between the strength of the potential field and distance is embedded in the potential theory's 'characteristic curve'. Polanyi assumed that the adsorption potential is independent of temperature. Hence, the characteristic curve can be generalized over a wide range of temperatures [4].

Shapiro and Stenby [10] adopted Polanyi's Potential theory and applied it to the modeling of multicomponent systems. In their MPTA framework, they integrate the solid-fluid potential, utilizing the Dubinin-Radushkevich-Astakhov (DRA) potential, with a fluid-fluid potential, using an equation of state, to describe the behavior of fluids both in the bulk and confined phases.Their MPTA-DRA model was used to model the confinement of different systems, pure components and mixtures, on activated carbon [11–13], molecular sieves [12], and metal-organic frameworks (MOFs) [14].

One great advantage of the MPTA model is its predictive power since it requires fitting to pure-component systems only and uses the fitted parameters to describe the adsorption of mixtures.

2.3 Molecular Simulation Studies

In the past few decades, MD and MC simulations have seen a surge in popularity in their use in modeling a variety of physical phenomena especially. Due to their rigorous theoretical foundations, molecular simulation methods have been utilized in the understanding the development of novel technologies. Recently, many researchers have used molecular simulation tools to understand and model adsorption phenomena. Severson and Snurr [15] studied the adsorption of n-alkanes in carbon slit pores using configurational-biased Grand Canonical Monte Carlo (GCMC) simulations. Other researchers looked into more realistic forms of adsorbents such as kerogen which is of great importance in the study and characterization of shale gas. Tesson and Firoozabadi [16] modeled the adsorption and diffusion behavior of methane in kerogen nanopores using a hybrid MD-GCMC model. In an attempt to model kerogen even more realistically, Pathak and Huang [17] studied the adsorption and absorption of fluids in a model of kerogen with active sites using a quasi-equilibrium MD simulation. Vasileiadis et al. [18] studied the adsorption of light alkanes and carbon dioxide in kerogen using GCMC simulations, employing 60 structures to represent the diverse void characteristics of kerogen. Besides modeling adsorption on kerogen, molecular simulation studies were carried out to study adsorption phenomena in zeolites [19–22] and metal-organic frameworks (MOFS) [23, 24].

2.4 Density Functional Theory Studies

DFT has been used in conjunction with molecular-based equations of state and molecular simulations to study the adsorption of a range of adsorbate-adsorbent

systems. For example, Liu et al. [25] studied the adsorption of alkanes in nanoslit graphite pores and their phase behavior under confinement utilizing the interfacial statistical theory of association fluids (iSAFT) and the Steele 10-4-3 potential. Peterson et al [26] studied the layering transitions within pores leading to capillary condensation using nonlocal DFT with GCMS. Sokolowski and Fischer [27] studied the adsorption of Lennard-Jones mixtures of Ar and Kr in narrow slit-like pores. The adsorption of polymeric mixtures was studied by Yu and Wu [28] by using Wertheim's first-order perturbation theory (TPT1) to model chain connectivity. While many researchers studied the thermophysical properties and phase behavior of fluids in confinement, others, such as Tripathi and Chapman [29], also focused on chemical reactions in porous media. Tripathi and Chapman studied the effects of confinement, such as that of capillary condensation, on reacting systems.

3. METHODOLOGY

Confined fluids, in this work, are assumed to lie within a potential field as put forth by Polanyi [9]. According to the potential theory, this field imposes a nonuniform distribution of molecules as one moves away from the adsorbent surface. In order to account for this nonuniform distribution, the system is discretized. The Helmholtz energy of the system is calculated as the sum of the Helmholtz energies of the constituent cells. The Helmholtz energy of each cell is calculated as the sum of two contributions: an internal contribution, which accounts for the fluid-fluid interactions and is calculated according to the SAFT-VR Mie EoS [30], and an external contribution, which accounts for the fluid-solid interactions and is calculated according to the MPTA model. In this work, the MPTA is implemented using two different adsorption models, namely, the Steele [31] and the DRA [32] potentials. Once the Helmholtz energy of the system is calculated, a minimization process is carried out to reach the state of thermodynamic equilibrium. Finally, once the system energy has been minimized, a Helmholtz-based stability test [1] is performed in each cell in order to detect phase-instability, which is an indicator of pore condensation.

3.1 System Geometry

In adsorption problems, the confined fluid exists in thermodynamic equilibrium with the bulk phase. Therefore, the total system energy has to be the sum of the two. In order to achieve that, the system is divided into regions, which are characterized by the presence, or lack thereof, of external fields. In the case of the confined region, further discretization into cells is needed to account for the nonuniform distribution of property values caused by the potential field. This discretization is done in the direction of the field being studied, in this case that is the potential field due to the

9
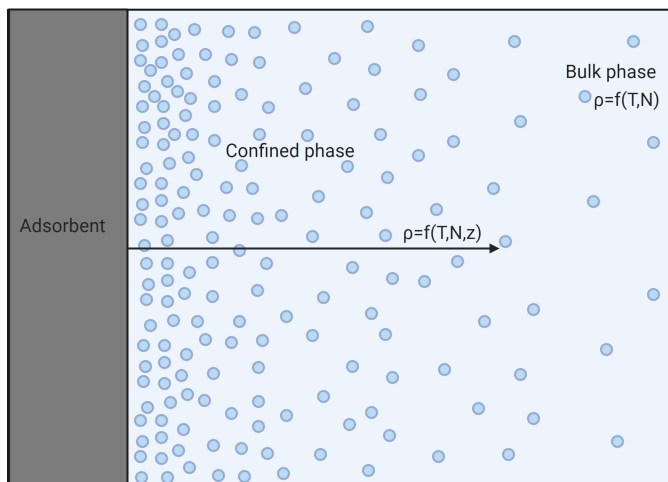
Figure 3.1: Nonuniform distribution of adsorbate molecules as a result of the potential field imposed by the adsorbent surface. Far from the pore wall, bulk properties are retained. Molecules are depicted as spheres for simplicity.

pore wall. Figure 3.1 can be used to visualize the the effect of the adsorbent surface on the adsorbate fluid.

In this work, it is assumed that all pores are slit-like and the pore walls are energetically homogeneous in the directions perpendicular to the potential field. This assumption simplifies the problem and allows for the treatment of multiple pores that are of the same size as though they are one. The pore volume of the system is translated into the volume of a single pore which extends in the two directions parallel to the surface of the wall. By doing that, the dimensionality of the problem is reduced from three to one. This can be justified based on the postulates of the potential theory which mandate a distribution of properties in one direction only which is the one perpendicular to the solid wall.

In this work, regions are denoted by the subscript m and grid cells, or layers, are denoted by the subscript j. Regions are characterized by the presence of the external potential field and the size of the pore. Therefore in order to simulate the setup of an

adsorption experiment, for example, one region, usually the one given index $m = 1$, represents the bulk phase while subsequent regions with indices $(m = 2, 3, ..., r)$ represent the adsorbed phases. The number of regions r is predefined based on the system being modeled. If the model is to simulate the equilibrium between a bulk phase and a matrix of pores of identical size and shape, then the number of regions defined is two; one for the bulk phase and one for the confined phase. By extension, the model can account for the presence of pores of different sizes and shapes by defining more confined regions. The total volume of the system, made up of bulk and confined regions, is constant and is equal to

$$V = \sum_{m=1}^{r} \sum_{j=1}^{l_m} V_{jm} \tag{3.1}$$

where l_m denotes the number of grid cells comprising region m. For the bulk phase, l_m is simply equal to 1. Figure 3.2 shows a schematic representation of the system geometry of a slit pore.

While this work only focuses on the effect of adsorption in slit-like pores, the model formulation is flexible enough to accommodate other types of fields, such as the gravitational, and other pore geometries, such as cylindrical and spherical. Moreover, more than one field and more than one field direction can be accommodated by extending the Helmholtz energy and discretizing the grid in different directions, respectively. For the scope of this work, the problem specifications are the temperature, number of moles of each component in the system and the volume of each region.

3.2   The Helmholtz Energy

The Helmholtz energy of the system A is the combination of the internal and external contributions which are calculated using the SAFT-VR Mie EoS and an
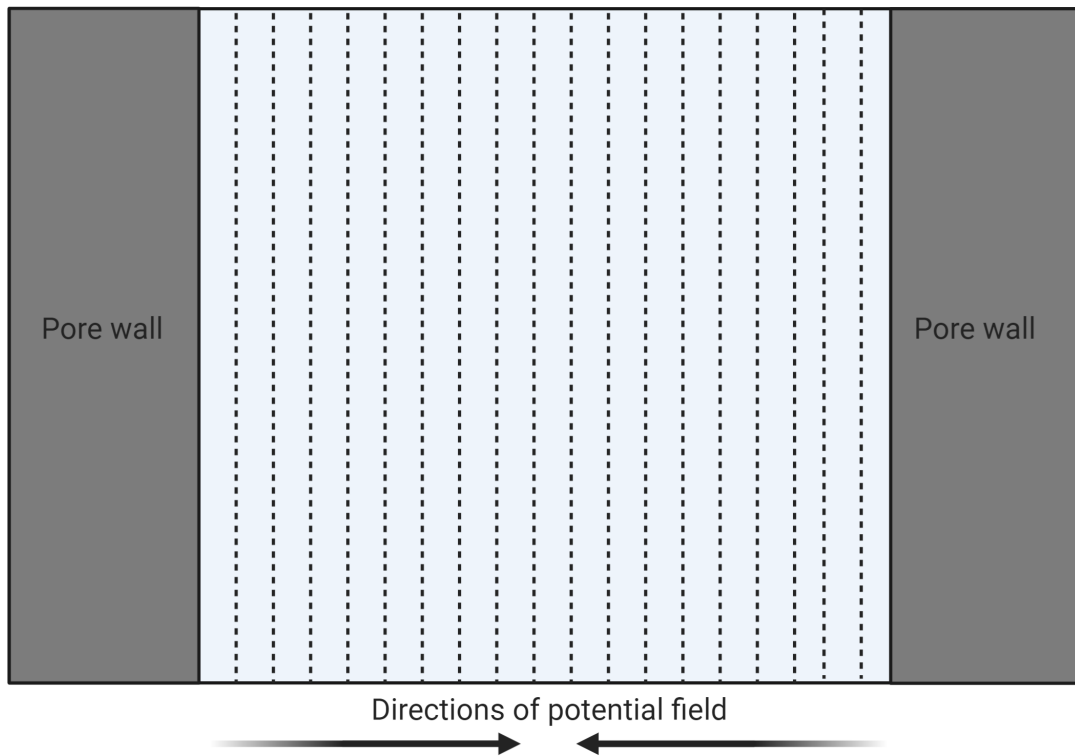
Figure 3.2: The volume confined by two parallel solid walls is divided into grid layers in the direction of the wall's potential field. Note the symmetry about the center of the pore.

adsorption model, respectively. In this section, the formulations used for the SAFT-VR Mie EoS and the Steele and DRA potentials will be discussed.

3.2.1   The SAFT-VR Mie Equation of State

Although this model can be used with virtually any equation of state that can accurately predict the thermodynamic behavior of the system, SAFT-VR Mie EoS is used due to its predictive power and wide range of applicability [30]. The Statistical Associating Fluid Theory for variable range interactions of the generic Mie form (SAFT-VR Mie) is a recent development in the SAFT family of equations of state. It is the based on Wertheim's first-order perturbation theory [30] and it treats molecules as spherical segments interacting through the Mie potential. The Mie potential is essentially a generalized Lennard-Jones potential with variable attractive and repulsive exponents. This variability gives the EoS predictive power for a lot of simple and complex fluids over a wide range of conditions. According to the basic formulation of the SAFT-VR Mie EoS, the dimensionless Helmholtz energy a is the sum of ideal-gas, monomer, chain and association contributions as shown in equation 3.2.

$$a = a^{ideal} + a^{mon} + a^{chain} + a^{assoc} \tag{3.2}$$

The dimensionless Helmholtz energy is defined as:

$$a = \frac{A\beta}{N_s} \tag{3.3}$$

where A is the Helmholtz energy, β is defined as $\beta = \frac{1}{kT}$, k is the Boltzmann constant, T is the absolute temperature and N_s is the number of monomeric segments defined as $N_s = m_s N$ and m_s is the number of segments per molecule and N is the number of molecules.

3.2.1.1 Ideal-Gas Term

The ideal-gas term is given by:

$$a^{ideal} = \left(\sum_{i=1}^{n} x_i \ln \rho_i \Lambda_i^3 \right) - 1 \tag{3.4}$$

where $x_i = N_i/N$ is the mole fraction of component i, $\rho_i = N_i/V$ is the molecular number density, N_i is the number of molecules of component i, n is the number of components in the mixture, and Λ_i is the de Broglie thermal wavelength of component i which comes from the statistical mechanical derivation of the partition function for an ideal gas [33].

3.2.1.2 Monomer Term

The monomer-segment contribution encapsulates the hard-sphere interactions between individual monomeric segments [30]. For a mixture, the monomer term is given by:

$$a^{mon} = \left(\sum_{i=1}^{n} x_i m_i \right) a^M \tag{3.5}$$

where a^M is the monomer's Helmholtz energy and it is calculated through a high-temperature expansion series truncated at the third term as follows:

$$a^M = a^{HS} + \beta a_1 + \beta^2 a_2 + \beta^3 a_3 \tag{3.6}$$

where a^{HS} is the Helmholtz energy of the reference hard-sphere and a_1, a_2, and a_3 are perturbation terms associated with the energy of attraction [30].

3.2.1.3 Chain Term

The Helmholtz energy associated with the formation of molecular chains from monomeric segments bonded tangentially is given by:

$$a^{chain} = -\sum_{i=1}^{n} x_i (m_i - 1) \ln g_{ii}^{Mie}(\sigma_{ii}) \tag{3.7}$$

where $g_{ii}^{Mie}(\sigma_{ii})$ is the radial distribution function RDF of Mie fluids evaluated at contact and σ_{ii} is the monomer-segment diameter of component i.

3.2.1.4 Association Term

The association contribution to the Helmholtz energy was obtained from the Wertheim first-order perturbation theory TPT1 and is given by:

$$a^{assoc} = \sum_{i=1}^{nc} x_i \sum_{a=1}^{s_i} \left[\ln X_{a_i} - \frac{X_{a_i}}{2} + \frac{1}{2} \right] \tag{3.8}$$

where the subscript a_i denotes the association site type and s_i denotes the number of association types present on component i, and X_{a_i} is the fraction of component i not bonded at sites a. The latter is defined as:

$$X_{a_i} = \frac{1}{1 + \rho \sum_{j=1}^{n} x_j \sum_{b=1}^{s_j} n_{b_j} X_{b_j} \Delta_{abij}} \tag{3.9}$$

where Δ_{abij} characterizes the association interaction strength between sites of type a on component i and sites of type b on component j. More discussion on the implementation of the association term and the solution for X_{ai} can be found in the work by Michelsen [34].

15

3.2.2 Adsorption Models

The external contribution to the Helmholtz energy is a function of the distance to the pore wall only. Using the MPTA implementation [10], the complete picture of solid-fluid-fluid interactions can be drawn by combining the mutually independent internal and external contributions. The two adsorption models used in this work are the Steele [31] and DRA [32] potentials.

3.2.2.1 The Steele Potential

The 10-4-3 Steele potential in this work is used to model the adsorption of fluids in slit-like pores consisting of two parallel walls. The Helmholtz energy of the adsorbate fluid is therefore calculated as:

$$A^f_{jm} = A^f_{jm}(z) + A^f_{jm}(H - z) \tag{3.10}$$

where A^f_{jm} is the Helmholtz energy due to the adsorption field which is calculated as the sum of the Helmholtz energies due to the two parallel walls and H is the wall-to-wall distance of the pore. Each of the two walls' contributions, represented by the two terms in Equation 3.10, can be calculated using Equation 3.11 with the difference being the distance z.

$$A^f_{jm}(z) = 2\pi\rho_s\Delta\sum_{i=1}^{\hat{c}} n_{ijm}\left[\varepsilon_{s,i}\sigma^2_{s,i}\left[\frac{2}{5}\left(\frac{\sigma_{s,i}}{z_{jm}}\right)^{10} - \left(\frac{\sigma_{s,i}}{z_{jm}}\right)^4 - \frac{\sigma^4_{s,i}}{3\Delta(0.61\Delta + z_{jm})^3}\right]\right] \tag{3.11}$$

Symbols ρ_s and Δ_s represent the density and inter-layer spacing of the adsorbent, respectively, $\epsilon_{s,i}$ and $\sigma_{s,i}$ are the energy and size parameters of the solid-fluid interaction, respectively, and they are calculated using the Lorentz-Berthelot combining rules [35].

16

$$\varepsilon_{s,i} = \left(\varepsilon_s \varepsilon_i\right)^{0.5} \tag{3.12}$$

$$\sigma_{s,i} = \frac{\sigma_s + \sigma_i}{2} \tag{3.13}$$

The subscripts s and i denote the properties of the solid and component i of the fluid mixture, respectively. The fluid parameters are obtained using the SAFT-VR Mie EoS whereas the solid parameters are fitted to adsorption experimental data.

3.2.2.2 The DRA Potential

The second adsorption potential used in this work is the DRA potential. The form of the potential utilized in this work is one modified by Shapiro and Stenby [10] to allow for the modeling of multicomponent mixtures and take into account the effect of heterogeneity of the adsorbate phase. Important to note, is that the DRA potential does not take into account the geometry of the pore, it merely correlates the pore volume with the energy of adsorption. However, the framework of this project has been based on the discretization of the pore volume therefore the Helmholtz energy due to the DRA potential can be calculated as:

$$A_{jm}^{*,f} = -\sum_{i=1}^{\hat{c}} n_{ijm}^* \left[\varepsilon_{0i} \left(\ln \left[\frac{H}{z_{jm}} \right] \right)^{1/\hat{\beta}} \right] \tag{3.14}$$

where ε_{0i} is the DRA energy parameter of component i and the exponent $\hat{\beta}$ is a parameter of the standard Dubinin-Radushkevich (DR) potential and it is equal to 2 for adsorption on activated carbon (AC) and 3 for that on molecular sieve (MS).

3.2.3   Stability Analysis

One major advantage of using MPTA to model the adsorption of fluids is that it allows for the detection of phase instability. Phase instability in the pore is an indicator of the occurrence of pore condensation. The stability analysis used in this work is A-GPhST [1].

The A-GPhST algorithm starts with the current equilibrium state of the system and seeks to find out whether the system's Helmholtz energy can be minimized further by the appearance of a new phase. The objective function in the A-GPhST calculations is the difference between the Helmholtz energy of the system and that of the same system with an added trial phase. The final form of the objective function, which was used in this work, is shown in the equation below:

$$\Omega_A = -\left(P^\bullet - P\right)\frac{V^\bullet}{RT} + \sum_{i=1}^{nc}\left(\frac{\mu_i^\bullet - \mu_i}{RT}\right)N_i^\bullet \tag{3.15}$$

where P, V, μ_i and N_i are the system's pressure, total volume, chemical potential of component i and number of moles of component i, respectively. The bullet superscript denotes the properties of the trial phase. This objective function is minimized using Newton's method. Once that is done, a conclusion can be made regarding the thermodynamic stability depending on the sign of the resulting objective function. This approach was adopted into this work by applying it on each cell of the grid. By doing that, one not only can detect the conditions of instability but can also narrow down the location of that instability within the pore.

3.3   Model Algorithm

In this section, a detailed description of the calculation steps followed in solving the model equations is presented.

First, inputs to the model, namely the temperature (T), volume of each region (V_m), and number of moles of each component in the system $(n_1, n_2, ..., n_n c)$ are defined, where the subscript nc is the number of components. In addition to these input variables, SAFT-VR Mie model parameters as well as solid-fluid potential parameters (based on the potential used in the calculation) are given as input.

Once the volume of each region is defined, the model creates the system geometry according to the details given in Section 3.1.

3.3.1   Initial Estimates

After defining the input and model variables and creating the system geometry, initial estimates for the number of moles in each grid cell of each region is calculated to be used in the subsequent Helmholtz minimization step. While the model allows flexibility in choosing the type of initial estimates, in this work the ideal gas law is used.

The initial estimates for the distribution of the number of moles is obtained from the funamental equilibrium equation

$$\frac{\mu_i^\alpha}{RT} = \frac{\mu_i^\beta}{RT} \tag{3.16}$$

where μ_i is the chemical potential of component i and the superscripts α and β represent the phases in equilibrium. In this work, the equilibrium condition applies among the chemical potentials of any component in all grid cells in all regions. To simplify the calculations, one grid cell is chosen to be the reference with which all other cells are in equilibrium. The reference grid cell is the one with the smallest potential field contribution.

Starting from Equation 3.16 and using the ideal gas law to calculate the internal contribution to the chemical potential, we find

19

$$\ln\left(x_i^\alpha P^\alpha\right) + \frac{\mu_i^{\alpha,f}}{RT} = \ln\left(x_i^\beta P^\beta\right) + \frac{\mu_i^{\beta,f}}{RT} \tag{3.17}$$

where x_i is the molar fraction of component i, the superscript f refers to the field contribution and P is the bulk pressure which, according to the ideal gas law, is defined as:

$$P^\alpha = \frac{n_{tot}^\alpha RT}{V^\alpha} \tag{3.18}$$

where n_{tot}^α is the total number of moles in phase α and V^α is the total volume of phase α. Upon combining and rearranging Equations 3.17 and 3.18, the following equation emerges:

$$\frac{n_i^\alpha}{V^\alpha} = \frac{n_i^\beta}{V^\beta} exp\left(\frac{\mu_i^{\beta,f} - \mu_i^{\alpha,f}}{RT}\right). \tag{3.19}$$

Equation 3.19 can then be generalized to calculate the number of moles in each grid cell. In order to simplify the calculations, the grid cell with the smallest potential field contribution is chosen as a reference cell, denoted by the subscript ref. The number of moles of component i in grid cell j of region m can then be calculated as follows:

$$\frac{n_{ijm}}{V_{jm}} = \frac{n_{i,ref}}{V_{ref}} exp\left(\frac{\mu_{i,ref}^f - \mu_{ijm}^f}{RT}\right). \tag{3.20}$$

Equation 3.20 is solved for each component in each grid cell, except the reference, yielding a system of $(nc(l_m - 1))$ linear equations. Adding to that (nc) equations for the conservation of the number of moles, defines as:

$$n_i = \sum_{m=1}^{r} \sum_{j=1}^{l_m} n_{ijm} \tag{3.21}$$

yields a system of $(nc \times l_m)$ linear equations which is sufficient to solve for the $(nc \times l_m)$ variables of the system.

3.3.2 Helmholtz Energy Minimization

Calculation of equilibrium properties requires the minimization of the Helmholtz energy of the system which is the sum of the internal and field contributions in all grid cells of all regions:

$$A = \sum_{m=1}^{r} \sum_{j=1}^{l_m} \left(A_{jm}^{int} + A_{jm}^{f} \right) \tag{3.22}$$

where A_{jm}^{int} is the internal contribution to the Helmholtz energy calculated using the SAFT-VR Mie EoS and A_{jm}^{f} is the field contribution to the Helmholtz energy calculated using the DRA or Steele potentials. The minimization is done using a second-order Newton's method modified based on Cholesky factorization, the details of which can be found in the work of Murray [36].

The Helmholtz energy minimization is done with respect to the number of moles in the system. A convenient alternative variable to the number of moles is the distribution factor θ_{ijm} which is defined as:

$$\theta_{ijm} = \frac{n_{ijm}}{n_i} \tag{3.23}$$

and it quantifies the distribution of any component i in the grids and regions of the system. The distribution factor is, by definition, a conserved quantity as shown in the following equation:

$$\sum_{m=1}^{r} \sum_{j=1}^{l_m} \theta_{ijm} = 1. \tag{3.24}$$

Due to the conservation of the number of moles, the number of independent variables is reduced from nc to $nc - 1$ for each grid in the system. Accordingly, the largest θ value of component i is taken to be the dependent variable, defined as:

$$\theta_{i,max} = 1 - (\sum_{m=1}^{r} \sum_{j=1}^{l_m} \theta_{ijm})_{\neq max} \tag{3.25}$$

At the beginning of each iteration and after calculating the initial estimates, the largest θ value is tagged as a dependent variable. Then, after calculating the independent θ values, the dependent θ is calculated again using equation 3.25. Having defined a dependent variable for each component, the total number of variables to be calculated becomes

$$n_{var} = nc \left(\left(\sum_{m=1}^{r} ml_m \right) - 1 \right) \tag{3.26}$$

where nc is the number of components, r is the number of regions and l_m is the number of grid cells in region m.

The minimization step requires the calculation of the gradient and Hessian which in turn require the first and second derivatives of the total Helmholtz energy with respect to the distribution factors, θ_{ijm}, as shown in the following equations:

$$\frac{\partial A}{\partial \theta_{ijm}} = n_i(\mu_{ijm} - \mu_{iJM}) \tag{3.27}$$

$$\frac{\partial^2 A}{\partial \theta_{i,j_i,m_i} \partial \theta_{k,j_k,m_k}} = n_i n_l \left[\left(\delta_{m_i,m_k} \delta_{j_i,j_k} - \delta_{m_i,M_k} \delta_{j_i,J_k} \right) \left(\frac{\partial \mu_{i,j_i,m_i}}{\partial \mu_{k,j_i,m_i}} \right) \right]$$
$$- n_i n_l \left[\left(\delta_{M_i,m_k} \delta_{J_i,j_k} - \delta_{M_i,M_k} \delta_{J_i,J_k} \right) \left(\frac{\partial \mu_{i,J_i,M_i}}{\partial \mu_{k,J_i,M_i}} \right) \right] \quad (3.28)$$

Lower-case subscripts denote the independent grid elements of components i and k whereas capital subscripts denote the dependent ones. The Greek letter δ represents the Kronecker delta function. The chemical potential of component i in grid layer j of region m is calculated as the sum of the internal and external contributions to the chemical potential as follows:

$$\mu_{ijm} = \left(\frac{\partial A_{jm}^{int}}{\partial n_{ijm}} \right)_{T,V_{jm},n_{\neq i,jm}} + \left(\frac{\partial A_{jm}^{f}}{\partial n_{ijm}} \right)_{T,V_{jm},n_{\neq i,jm}} . \quad (3.29)$$

Once the minimization process converges, which is achieved when the norm of the gradient vector is equal to zero within a predefined tolerance, thermodynamic properties of the system are calculated.

3.3.3   Phase Stability Test and Phase Addition

Although the minimization step ensures that the system reaches thermodynamic equilibrium, it does not take into consideration the possibility of phase change. This is where the phase stability test comes in. It ensures that the system is at its global energy minimum taking into account the possibility of the appearance of a new phase.

If the pressure of a grid layer is negative, then the layer is automatically considered unstable and the purpose of running the stability test is to generate initial estimates for the new phase. If the pressure in the grid layer is positive, the stability test is used to reach a conclusion about its phase stability. If the conclusion is that the grid

layer is unstable, the stability test generates initial estimates for the added phase. The steps below give an outline of the stability test employed in this work:

1. Initial estimates for the trial phase are calculated using the composition of the vapor phase at the bubble point calculated using Raoult's law with the pure component vapor pressures calculated using the Wilson correlation [37] according to Michelsen's formulation [38].

2. The trial phase's initial estimate of the composition, along with the system temperature and pressure, is used to calculate the vapor-like density root by employing Topliss' root-finding algorithm [39].

3. The density root is then used to calculate the number of moles of each component in the trial phase.

4. The resulting number of moles is then used as an initial estimate for the second-order minimization of the Helmholtz-based objective function, shown in Equation 3.15.

5. If the minimum of objective function $\Omega_{A,min}$ is found to be positive, i.e. the phase is stable, the same preceding steps are repeated now with a liquid phase composition as the initial estimate.

6. If $\Omega_{A,min}$ is found to be negative, i.e. the phase is unstable, for either the vapor or liquid phase initial estimates, the grid layer is tagged as unstable and the model proceeds to phase addition.

Once the stability test concludes that the grid layer is unstable and generates initial estimates for the composition and density of the new phase, a series of calculations, highlighted in the following steps, begin to add a new phase within the grid layer:

24

1. The initial estimate for the density of the new phase is compared with the two adjacent layers on either side of the one which was just tagged as unstable. This is done to decide on the location of the new added phase; it is added near the adjacent layer with a comparable density value.

2. The new phase is allocated a volume with the original unstable layer which will ensure that the number of moles allocated for the new phase does not exceed that of the original layer. Let the volume fraction γ be defined as the fraction of the original layer given to the new phase. In order to ensure the total number of moles in the new phase does not exceed the number of moles in the original layer, the following relationship is to be satisfied:

$$n_{jm}^{\bullet} = \gamma \rho_{jm}^{\bullet} V_{jm} < n_{jm} \qquad (3.30)$$

where $n_{jm}^{\bullet}$ is the total number of moles given to the new phase, $\rho_{jm}^{\bullet}$ is an initial estimate of the molar density of the new phase as calculated in the stability test and V_{jm} and n_{jm} are the volume and number of moles in the original grid layer j or region m. After rearranging, the variable γ can be defined as

$$\gamma = f\left(\frac{\rho_{jm}}{\rho_{jm}^{\bullet}}\right) \qquad (3.31)$$

where f is an arbitrary coefficient with a value greater than 0 and less than 1.

3. Once the volume for the new phase has been allocated, the initial estimate for the number of moles of each component in the new phase is calculated as follows:

$$n_{ijm}^{k+1} = \alpha x_{ijm}^{\bullet} n_{jm}^{k} \qquad (3.32)$$

where α is a small numerical factor of the order of magnitude of 10^{-4} and $x_{ijm}^{\bullet}$ is the initial estimates for the mole fraction of component i as calculated in the stability test. The superscript k represents the value of the variable after the last Helmholtz minimization whereas $k+1$ represents the value of the variable in the current minimization step.

4. Once the new phase is added and the initial estimates for the number of moles are calculated, the Helmholtz minimization step, described in Section 3.3.2, is performed again.

3.4   Code Development

The set-up of the geometry and the minimization calculations carried out to solve this model were run on a FORTRAN code. Subroutines responsible for the calculation of intermediate variables of the SAFT-VR Mie EoS and the adsorption models were written using Mathematica and converted to Fortran subroutines using the Thermath package [40].

4. RESULTS AND DISCUSSION

In this chapter, results of the MPTA-SAFT-VR Mie model are presented. As discussed beforehand, in any calculation, the fluid-fluid interactions are described using the SAFT-VR Mie EoS whereas the solid-fluid interactions are described using either of the two solid-fluid potentials, namely Steele or DRA. The EoS parameters used in this work are obtained from Lafitte et al. [30] and Dufal et al. [41] and are summarized in Table 4.1.

Table 4.1: SAFT-VR Mie molecular parameters [30, 41].

Component	m_i	$\sigma(\mathring{A})$	$\epsilon/k(K)$	λ_r	λ_a
CH_4	1.0000	3.7412	153.360	12.6500	6.0
N_2	1.4214	3.1760	72.438	9.8749	6.0
CO_2	1.6936	3.0465	235.73	18.067	6.0
C_2H_6	1.7230	3.4763	164.27	10.121	6.0
C_2H_4	1.7972	3.2991	142.64	9.6463	6.0
iC_4H_{10}	1.7186	4.2177	281.12	14.612	6.0

In this table, σ is the size parameter representing the monomeric segment diameter of the fluid, ϵ is the depth of the potential well and λ_r and λ_a are the repulsive and attractive exponents, respectively, of the generalized Lennard Jones potential equation.

Steele potential parameters were obtained from Li et al. [42] using DFT with a volume-translated Peng-Robinson EoS and are summarized in Table 4.2.No need arose to reparameterize the model using the SAFT-VR Mie EoS due to the almost exact agreement between results of this work and results reported by Dawass et al. [2]

who used the same framework as the one used here but with the PR EoS instead of the SAFT-VR Mie EoS.

Table 4.2: Steele potential parameters [42].

Parameter	Value	Units
ε_{CH_4}/k	1178	K
ε_s/k	20	K
σ_s	3.345×10^{-10}	m
Δ_m	3.35×10^{-10}	m
ρ_s	1.14×10^{29}	m^{-3}

The DRA potential parameters used in this work were obtained by fitting the experimental pure component adsorption isotherms of methane, nitrogen and carbon dioxide collected by Dreisbach et al. [43]. The volume parameter v_0 is adsorbent-specific and therefore was fitted to all three adsorption isotherms whereas the energy parameters ε_{i0} are fluid-specific. The DRA parameters are shown in Table 4.3.

Table 4.3: DRA-SAFT-VR Mie model parameters

Component	Adsorbent	$\hat{\beta}$	v_0 (m^3/kg)	ε_{i0} (kJ/mol)
CH_4				7.492
N_2	AC	2	4.257×10^{-4}	5.569
CO_2				7.342
C_2H_6				12.934
iC_4H_{10}				19.556
C_2H_4	MS	3	1.556×10^{-4}	18.454
CO_2				17.952

Besides the fluid-fluid and solid-fluid parameters listed, no binary interaction

parameters were used in the modeling of mixture adsorption.

4.1 Steele Potential Results

The adsorption of methane was modeled using the Steele potential with the SAFT-VR Mie EoS and compared to results of DFT calculations by Li et al. [42] and MPTA-Peng-Robinson calculations by Dawass et al. [2].

First, adsorption in a single slit-like pore is modeled. Methane adsorbed on a single AC pore with a wall-to-wall distance of $H = 2$ nm at 298 K is modeled at three different bulk pressure values, namely 0.1 MPa, 1 MPa and 2 MPa. The resulting Figure 4.1 shows the local density profile of methane within the pore at the three aforementioned bulk pressures. The results of this work are plotted alongside results of the MPTA-PR as implemented by Dawas et al. [2].

As can be seen in Figure 4.1, the density is zero near the wall due to size exclusion between the atoms of the solid adsorbent and the methane molecules. The density peaks at around 0.3 nm which is the distance at which the solid-fluid attraction is at its maximum. As the distance increases beyond that, the density quickly drops to a near-constant value at the center of the pore at 1 nm. Due to the symmetry of the pore about the center, only half of the density profile is shown, since the right-hand side is an exact mirror image of the left-hand side. It is clear that as the bulk pressure increases, the amount of fluid adsorbed in the pore also increases as evident in the upward shift and widening of the adsorption isotherm. The results of this work show excellent agreement with results of the MPTA-PR model implemented by Dawas et al. [2].

Besides the effect of bulk pressure on adsorption, the effect of varying pore size was modeled. Figure 4.2, shows the adsorption of methane on AC at 303.15 K in three different pore sizes, namely 2, 3 and 6 nm. Results are plotted alongside DFT
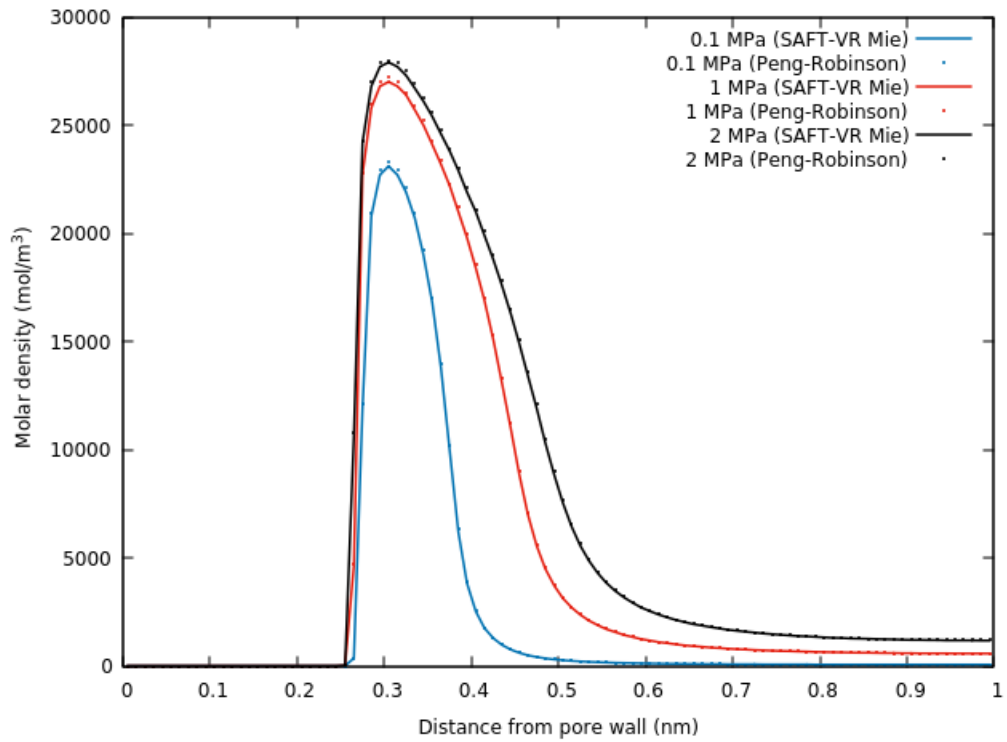
Figure 4.1: Local density profiles for CH_4 at 298 K and H= 2 nm. The SAFT-VR Mie EoS results are produced in this work and the volume-translated Peng-Robinson EoS results were produced by Dawass et al. [2]
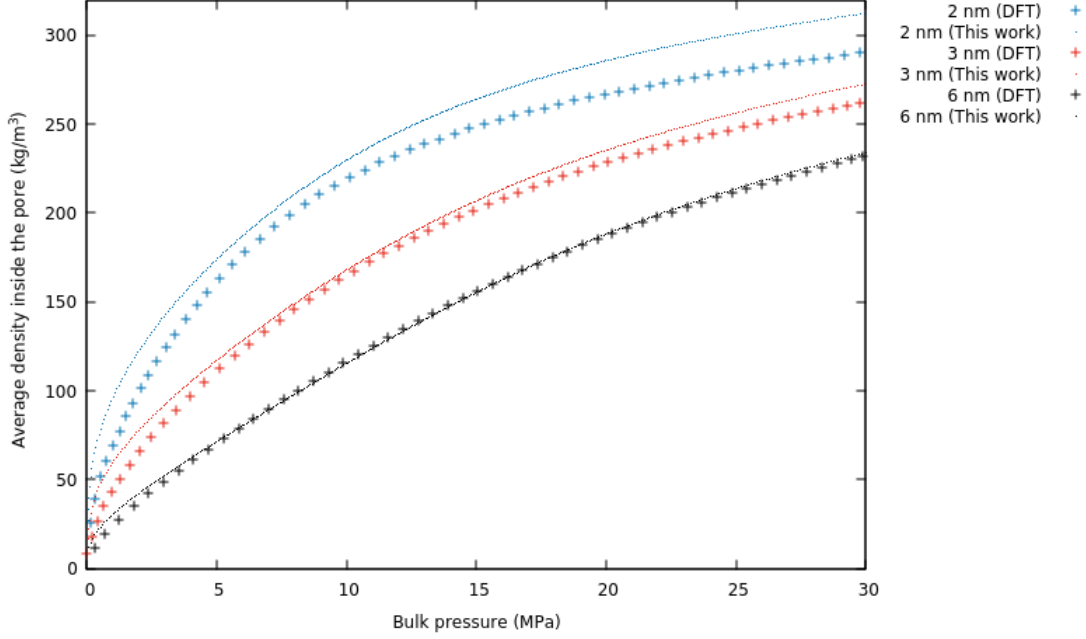
Figure 4.2: CH_4 adsorption isotherm at 303.15 K for three pore widths. Dashed lines are results of this work and cross symbols are DFT calculation results by Li et al. [42]

calculations by Li et al. [42].

The density in Figure 4.2 is defined as the average density across the pore normalized with the pore width as follows:

$$\rho_{im} = \frac{1}{H_{in,m}} \int_0^{H_m} \rho_{im}(z_m) dz_m \tag{4.1}$$

where ρ_{im} is the average density of component i in region m, $H_{in,m}$ is the wall-to-wall distance of the pore minus the the diameter of the adsorbed molecule and H_m is the pore's total wall-to-wall distance. Due to the system geometry employed in this work, the averaging for the density is done using a sum over grid layers instead of integrating over the distance from the wall. So Equation 4.1 becomes:

$$\rho_{im} = \frac{H_m \sum_{j=1}^{l_m} n_{ijm}}{H_{in,m} V_m}. \qquad (4.2)$$

Results of the MPTA-SAFT-VR Mie model show good agreement with the DFT calculation results with increasing deviation at high pressure and in small wall-to-wall separations. It can be shown that as the pore size increases, the average density within the pore decreases. This can be attributed to the fact that the local density within the pore decreases as the distance to the wall increases which means that larger pores adsorb fewer molecules per unit wall-to-wall separation than smaller pores. This in turn is because a larger fraction of the volume of larger pores experiences weaker attraction to the walls.

In some cases it is not sufficient to treat the pores within a porous medium as being uniform in size and therefore incorporating a pore size distribution (PSD) into the calculations becomes necessary. Low-pressure adsorption of methane at 363 K in an AC with a PSD, shown in Table 4.4, was modeled using a 6-pore-size approximation as shown in Figure 4.3. The size heterogeneity was represented by using multiple regions; one for each pore size bin. The 6 pore sizes with the largest contribution to the pore volume were chosen, neglecting pore sizes with relatively small total volume. The results of this work are shown alongside experimental data collected by Qiao et al. [44]. The volume of each region representing each pore size in the distribution was calculated according to the work of Dawass et al. [2].

Table 4.4: Pore size distribution [?]

H_m / nm	PSD / m³·kg^{-1}·nm^{-1})	V_m / m³·kg^{-1})
0.8	3.03E-06	3.82E-06
0.9	7.33E-05	2.38E-05
1.0	4.03E-04	6.34E-05
1.1	8.65E-04	9.29E-05
1.2	9.93E-04	8.65E-05
1.3	7.37E-04	5.70E-05
1.4	4.02E-04	2.89E-05
1.5	1.75E-04	1.20E-05
1.6	6.46E-05	4.29E-06
1.7	2.11E-05	1.37E-06
1.8	6.28E-06	4.01E-07
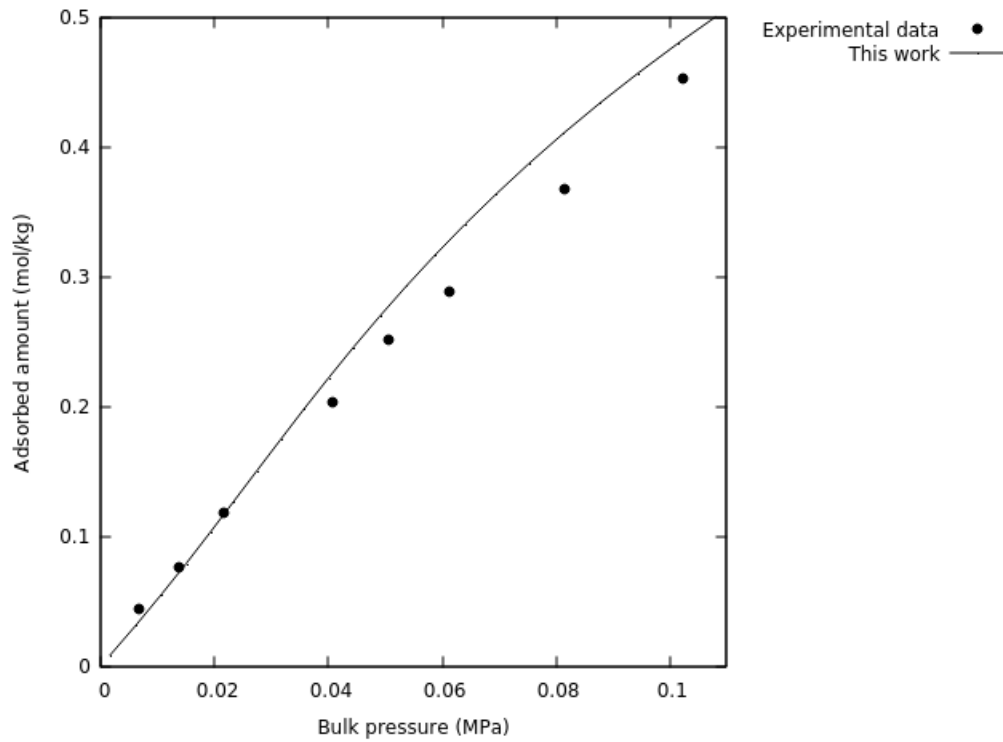
Figure 4.3: CH_4 adsorption isotherm at 363.15 K using a 6-pore-size approximation to the PSD. Results of ths work are compared with experimental data points by Qiao [44]

4.2 DRA Potential Results

The DRA potential was used to model the adsorption of methane, nitrogen, carbon dioxide and their mixtures on AC and mixtures of ethane, ethylene, isobutane and carbon dioxide on MS. The two adjustable parameters for the DRA potential, v_0 and ε_{i0}, were obtained by fitting pure component adsorption isotherms of the different components. Mixture adsorption was then predicted using those pure component parameters. Table 4.3 shows the DRA parameters obtained in this work.

Adsorption isotherms in this section are represented in terms of the surface excess (Γ) and absolute adsorbed amounts (N^{ads}). The surface excess (also known as the Gibbs excess) is a measure of the difference between the amount of fluid adsorbed and the amount remaining in the bulk phase and it is defined as follows:

$$\Gamma_i = \int_0^H (\rho(z)x_i(z) - \rho_B x_{Bi})dz \tag{4.3}$$

where $\rho(z)$ is the overall density of fluid at distance z from the wall, $x_i(z)$ is the mole fraction of component i of the fluid at distance z and the subscript B denotes the property at the bulk phase. Due to the way the discretization of the system used in this work, the excess surface is calculated as:

$$\Gamma_{im} = \left(\sum_{j=1}^{l_m} n_{ijm}\right) - V_m \rho_B x_{Bi}. \tag{4.4}$$

The absolute adsorbed amount N_i^{abs} of component i is defined as:

$$N_{im}^{ads} = \sum_{j=1}^{l_m} n_{ijm}. \tag{4.5}$$

.

In the case of mixture adsorption, mole fractions are used to quantify the relative

adsorption of each component with respect to the other components. The surface excess mole fraction of component i in region m is thus defined as:

$$x_{im}^{ex} = \frac{\Gamma_{im}}{\sum\limits_{i=1}^{nc} \Gamma_{im}}.$$

(4.6)

Similarly, the absolute adsorbed mole fraction of component i in region m is defined as:

$$x_{im}^{ads} = \frac{N_{im}^{ads}}{\sum\limits_{i=1}^{nc} N_{im}^{ads}}.$$

(4.7)

Because the DRA potential does not depend on the geometry of the system and the heterogeneity of pores, the DRA calculations in this work were performed using one representative confined region.

Figures 4.4, 4.5 and 4.6 show the adsorption isotherms of methane, nitrogen and carbon dioxide, respectively, at 298 K alongside experimental data points reported by Dreisbach et al. [43]. Results show excellent agreement with experimental data in the cases of methane and carbon dioxide with more deviation observed in the case of nitrogen.
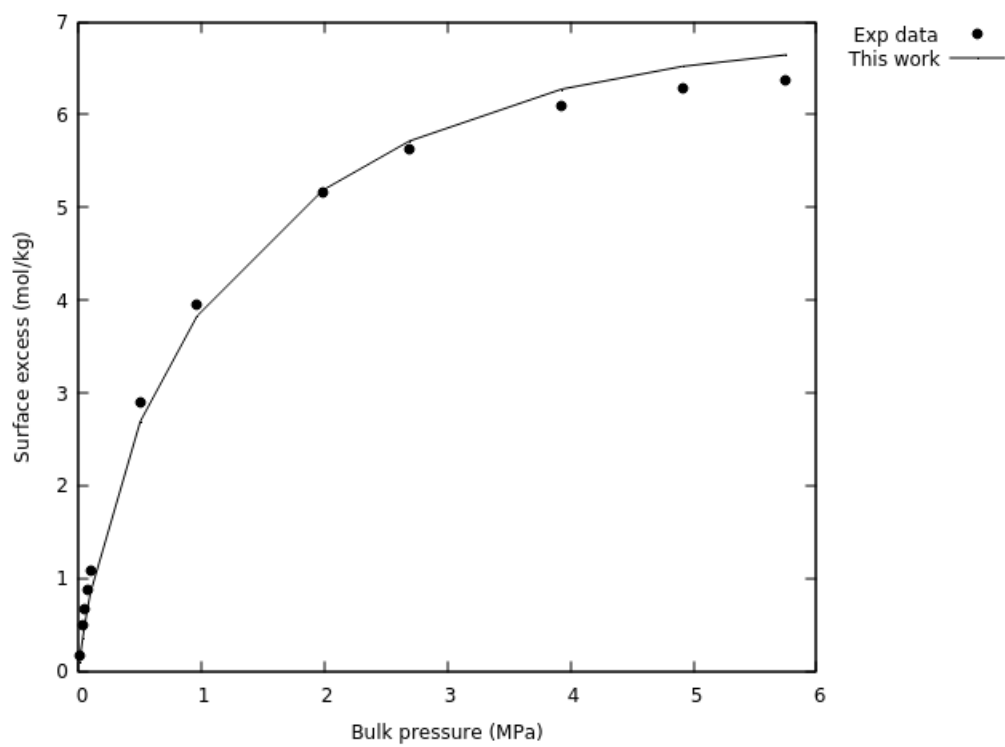
Figure 4.4: Adsorption isotherms of CH_4 on AC. Results are compared with experimental data points by Dreisbach et al. [43]
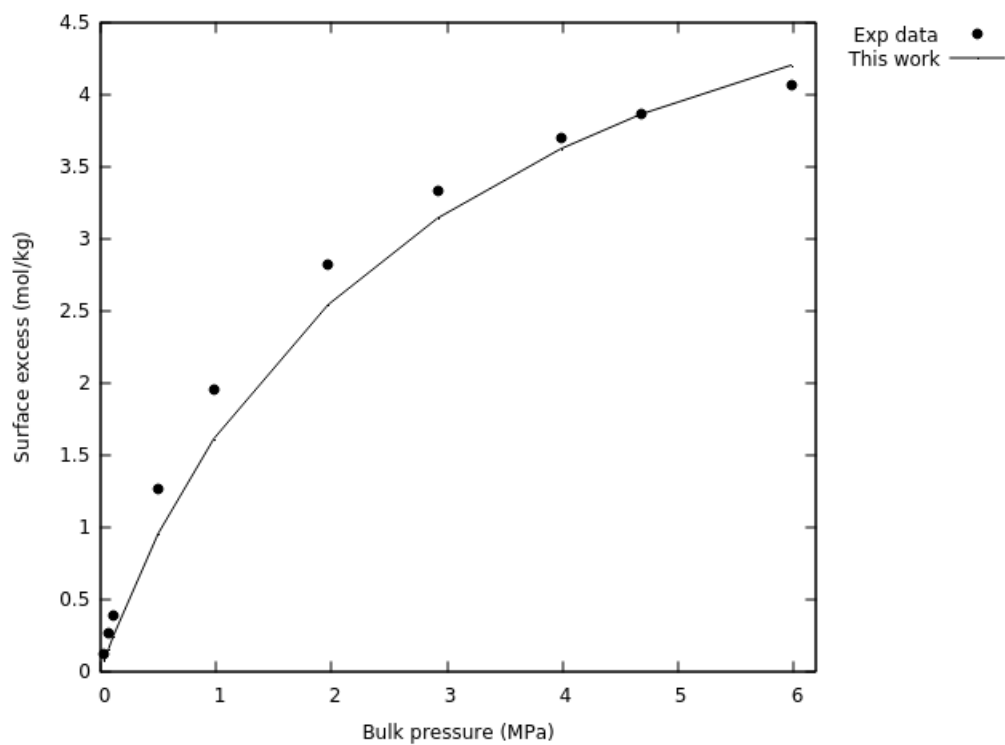
Figure 4.5: Adsorption isotherm of N_2 at 298 K. Experimental data points were obtained by Dreisbach [43]
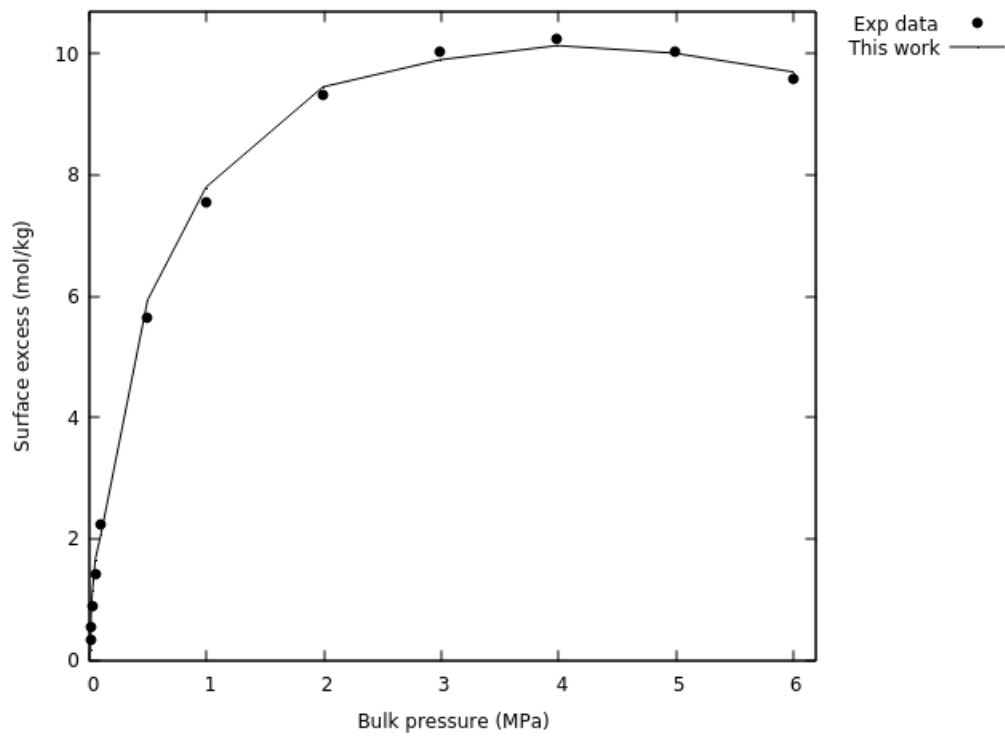
Figure 4.6: Adsorption isotherm of CO_2 at 298 K. Experimental data points were obtained by Dreisbach [43]

The adsorption of binary mixtures of CH_4, N_2 and CO_2 was calculated at 298 K and at varying values of the bulk composition and compared to the experimental data of Dreisbach et al. [43]. The full calculation results for the binary adsorption equilibria are presented in Tables A.1 - A.6 in the appendix. Ternary-mixture adsorption equilibria was also predicted for mixtures of three aforementioned components of varying bulk-phase composition. Similar to the calculations of binary mixture adsorption, ternary mixture adsorption was predicted using the energy parameter (ε) of pure components fitted to experimental pure component adsorption isotherms. The absolute and surface excess adsorption equilibrium results for the ternary mixtures of methane-nitrogen-carbon dioxide can be found in Tables A.7 and A.8 in the appendix.

Binary mixture adsorption of C_2H_6, C_2H_4, iC_4H_{10} and CO_2 on MS was similarly predicted, using pure-component parameters, at a bulk-phase pressure of 0.1378 MPA and at varying bulk-phase compositions and several temperature values. The results of the model predictions are shown in Tables A.9 - A.11.

In order to quantify the accuracy of the model's predictions, percent average absolute deviation values were calculated for the total absolute adsorbed amounts ($AAD_n\%$) and for the mole fraction of absolute adsorbed amounts ($AAD_x\%$) as follows:

$$AAD_n\% = \frac{100}{n_{exp}} \sum_{k=1}^{N_{exp}} |\frac{N_{ads}^{exp,k} - N_{ads}^{calc,k}}{N_{ads}^{exp,k}}| \tag{4.8}$$

$$AAD_x\% = \frac{100}{n_{exp}} \sum_{k=1}^{N_{exp}} |x_i^{exp,k} - x_i^{calc,k}| \tag{4.9}$$

where n_{exp} is the number of experimental data points. Table 4.5 summarizes the average absolute deviations for this work alongside those of the MPTA-SRK and

MPTA-SBWR [12]. Overall, the MPTA-SAFT-VR Mie model yields good agreement with experimental data and comparable performance with the other two models reported in the case of adsorption on AC. In the case of adsorption on MS, the model performs significantly better than the MPTA-SBWR and generally slightly better than the MPTA-SRK. Even though this model yields results of relatively comparable accuracy to models which employ simpler EoS, the advantage of implementing the SAFT-VR Mie EoS instead of a cubic EoS lies in its potential in yielding accurate results for complex systems, such as systems which contain associating components. Although this work does not include the adsorption of associating systems, a significant improvement in its performance, relative to the other models, can be observed going from simple light-gas systems to hydrocarbon components of longer chains. Such trend is to expected when moving to even more complex systems.

Table 4.5: Average absolute deviations for the mixture adsorptions

Mixture	Data Points	DRA + SAFT-VR Mie		DRA + SRK [12]		DRA + SBWR [12]		Data Reference
		$AAD_x\%$	$AAD_n\%$	$AAD_x\%$	$AAD_n\%$	$AAD_x\%$	$AAD_n\%$	
$CH_4 + N_2$	24	4.12	10.36	2.52	4.45	1.47	7.12	
$CH_4 + CO_2$	24	4.50	6.38	4.2	7.39	5.91	8.71	[43]
$CO_2 + N_2$	24	2.63	7.34	3.75	7.89	4.32	8.56	
$CH_4 + N_2 + CO_2$	40	10.36	8.58	17.47	9.38	21.61	10.80	
Total	112	5.4	8.16	6.99	7.28	8.33	8.80	
$C_2H_6 + iC_4H_{10}$	17	5.73	5.84	7.72	7.55	9.27	7.28	
$C_2H_4 + iC_4H_{10}$	24	5.31	4.22	10.14	3.70	13.73	33.4	[45]
$C_2H_4 + CO_2$	11	4.26	5.47	3.57	6.00	4.52	0.60	
Total	52	5.10	5.18	7.14	5.75	9.17	13.76	

5. CONCLUSIONS AND FUTURE WORK

In this work, an adsorption model based on the Multi-component Potential Theory of Adsorption and the SAFT-VR Mie EoS was adopted to model the adsorption of light gases and their mixtures on activated carbon. With the problem specifications being the temperature, volume and number of moles of the system, the objective function minimized is the Helmholtz energy. Solid-fluid interactions were accounted for using the Steele and DRA potentials. Results show excellent agreement with experimental data as well as DFT calculations. The model used in this work has the modularity that enables it to deal with various problems. The flexibility in defining the system geometry allows for the treatment of heterogeneous adsorbents by assigning multiple confined regions with distinct pore sizes and adsorption energies. Additionally, the model allows for the treatment of various pore geometries such as cylindrical and spherical without much change to the overall structure or algorithm. Additional fields, besides the potential field due to the confining pore, can be incorporated such as the work by Dawass et al. [2] which describes the behavior of fluids under the effect of both confinement and compositional grading due the gravitational field.

Even though the SAFT-VR Mie EoS is more computationally demanding than simple cubic EoS, the advantage of employing it in this work lies in its ability to accurately predict the thermophysical properties and phase equilibrium behavior of more complex fluid systems. Based on that, the adsorption of associating fluids will be the topic of focus in the near future. In addition to the adsorption of associating fluids, future work will include adsorption isotherm calculations for cases which exhibit capillary condensation using the Helmholtz-based stability test discussed and

implemented in this work.

REFERENCES

[1] M. Castier, "Helmholtz function-based global phase stability test and its link to the isothermal-isochoric flash problem," *Fluid Phase Equilibria*, vol. 379, pp. 104–111, 2014.

[2] N. Dawass, M. L. D'Lima, I. G. Economou, and M. Castier, "Phase Equilibrium with External Fields: Application to Confined Fluids," *Journal of Chemical and Engineering Data*, vol. 61, no. 8, pp. 2873–2885, 2016.

[3] I. Langmuir, "The Adsorption of Gases on Plane Surfaces of Glass, Mica and Platinum," *Journal of the American Chemical Society*, vol. 40, no. 9, pp. 1361–1403, 1918.

[4] A. Dabrowski, "Adsorption - from theory to practice," *Advances in Colloid and Interface Science*, vol. 93, no. 1–3, pp. 135–224, 2001.

[5] A. W. Adamson and A. P. Gast, *Physical Chemistry of Surfaces*. California: John Wiley Sons Inc., 6 ed., 1997.

[6] R. Sips, "On the Structure of a Catalyst Surface. II," *The Journal of Chemical Physics*, vol. 18, no. 1948, p. 1024, 1950.

[7] J. Toth, "Uniform Interpretation of Gas/Soild Adsorption," *Advances in Colloid and Interface Science*, vol. 55, pp. 1–239, 1995.

[8] S. Brunauer, P. H. Emmet, and E. Teller, "Adsorption of Gases in Multimolecular Layers," *Journal of American Chemical Society*, vol. 60, no. 2, pp. 309–319, 1938.

[9] M. Polanyi, "Theories of the adsorption of gases. A general survey and some additional remarks.," *Transactions of the Faraday Society*, vol. 28, pp. 316–333, 1932.

[10] A. A. Shapiro and E. H. Stenby, "Potential Theory of Multicomponent Adsorption," *Journal of Colloid and Interface Science*, vol. 201, pp. 146–157, may 1998.

[11] M. A. Monsalvo and A. A. Shapiro, "Study of high-pressure adsorption from supercritical fluids by the potential theory," *Fluid Phase Equilibria*, vol. 283, pp. 56–64, sep 2009.

[12] M. A. Monsalvo and A. A. Shapiro, "Modeling adsorption of binary and ternary mixtures on microporous media," *Fluid Phase Equilibria*, vol. 254, no. 1-2, pp. 91–100, 2007.

[13] E. Dundar, R. Zacharia, R. Chahine, and P. Bénard, "Modified potential theory for modeling supercritical gas adsorption," *International Journal of Hydrogen Energy*, vol. 37, pp. 9137–9147, 2012.

[14] E. Dundar, R. Zacharia, R. Chahine, and P. Bénard, "Potential theory for prediction of high-pressure gas mixture adsorption on activated carbon and MOFs," *Separation and Purification Technology*, vol. 135, pp. 229–242, 2014.

[15] B. L. Severson and R. Q. Snurr, "Monte Carlo simulation of n-alkane adsorption isotherms in carbon slit pores.," *The Journal of Chemical Physics*, vol. 126, p. 134708, apr 2007.

[16] S. Tesson and A. Firoozabadi, "Methane adsorption and self-diffusion in shale kerogen and slit nanopores by molecular simulations," *The Journal of Physical Chemistry C*, vol. 122, no. 41, pp. 23528–23542, 2018.

[17] M. Pathak, H. Kweon, M. Deo, and H. Huang, "Kerogen swelling and confinement: its implication on fluid thermodynamic properties in shales," *Scientific reports*, vol. 7, no. 1, pp. 1–14, 2017.

[18] M. Vasileiadis, L. D. Peristeras, K. D. Papavasileiou, and I. G. Economou, "Transport properties of shale gas in relation to kerogen porosity," *The Journal of Physical Chemistry C*, vol. 122, no. 11, pp. 6166–6177, 2018.

[19] B. Smit and J. I. Siepmann, "Simulating the adsorption of alkanes in zeolites," *Science*, vol. 264, no. 5162, pp. 1118–1120, 1994.

[20] J. P. Fox and S. P. Bates, "Simulating the adsorption of binary and ternary mixtures of linear, branched, and cyclic alkanes in zeolites," *The Journal of Physical Chemistry B*, vol. 108, no. 44, pp. 17136–17142, 2004.

[21] A. H. Fuchs and A. K. Cheetham, "Adsorption of guest molecules in zeolitic materials: computational aspects," 2001.

[22] A. Gupta, L. A. Clark, and R. Q. Snurr, "Grand canonical monte carlo simulations of nonrigid molecules: siting and segregation in silicalite zeolite," *Langmuir*, vol. 16, no. 8, pp. 3910–3919, 2000.

[23] T. Düren, L. Sarkisov, O. M. Yaghi, and R. Q. Snurr, "Design of new materials for methane storage," *Langmuir*, vol. 20, no. 7, pp. 2683–2689, 2004.

[24] H. Frost, T. Düren, and R. Q. Snurr, "Effects of surface area, free volume, and heat of adsorption on hydrogen uptake in metal- organic frameworks," *The Journal of Physical Chemistry B*, vol. 110, no. 19, pp. 9565–9570, 2006.

[25] J. Liu, L. Wang, S. Xi, D. Asthagiri, and W. G. Chapman, "Adsorption and phase behavior of pure/mixed alkanes in nanoslit graphite pores: an isaft application," *Langmuir*, vol. 33, no. 42, pp. 11189–11202, 2017.

[26] B. K. Peterson, G. S. Heffelfinger, K. E. Gubbins, and F. van Swol, "Layering transitions in cylindrical pores," *The Journal of chemical physics*, vol. 93, no. 1, pp. 679–685, 1990.

[27] S. Sokolowski and J. Fischer, "Lennard-jones mixtures in slit-like pores: a comparison of simulation and density-functional theory," *Molecular Physics*, vol. 71, no. 2, pp. 393–412, 1990.

[28] Y.-X. Yu and J. Wu, "Density functional theory for inhomogeneous mixtures of polymeric fluids," *The Journal of chemical physics*, vol. 117, no. 5, pp. 2368–2376, 2002.

[29] S. Tripathi and W. G. Chapman, "A density functional approach to chemical reaction equilibria in confined systems: application to dimerization," *The Journal of chemical physics*, vol. 118, no. 17, pp. 7993–8003, 2003.

[30] T. Lafitte, A. Apostolakou, C. Avendano, A. Galindo, C. S. Adjiman, E. A. Muller, and G. Jackson, "Accurate statistical associating fluid theory for chain molecules formed from Mie segments," *The Journal of Chemical Physics*, vol. 139, no. 15, p. 154504, 2013.

[31] W. A. Steele, "The Physical Interaction of Gases with Crystalline Solids I. Gas-Solid Energies and Properties of Isolated Adsorbed Atoms," *Surface Science*, vol. 36, pp. 317–352, 1973.

[32] M. M. Dubinin, "Generalization of the Theory of Volume Filling of Micropores to Nonhomogeneous Microporous Structure," *Carbon*, vol. 23, no. 4, pp. 373–380, 1985.

[33] S. I. Sandler, *An Introduction to Applied Statistical Thermodynamics*. Wiley & Sons, 2011.

[34] M. L. Michelsen, "Robust and Efficient Solution Procedures for Association Models," *Industrial and Engineering Chemistry Research*, vol. 45, no. 25, pp. 8449–8453, 2006.

[35] W. B. Brown, "The statistical thermodynamics of mixtures of lennard-jones molecules i. random mixtures," *Philosophical Transactions of the Royal Society of London. Series A, Mathematical and Physical Sciences*, vol. 250, no. 976, pp. 175–220, 1957.

[36] W. Murray, "Second Derivative Methods," in *Numerical Methods for Unconstrained Optimization*, pp. 57–71, London: Academic Press, 1972.

[37] G. Wilson, "A modified redlich-kwong equation of state applicable to general physical data calculations," in *AIChE Meeting, Paper*, no. 15C, 1968.

[38] M. L. Michelsen, "The isothermal flash problem. part i. stability," *Fluid phase equilibria*, vol. 9, no. 1, pp. 1–19, 1982.

[39] R. J. Topliss, D. Dimitrelis, and J. M. Prausnitz, "Computational aspects of a non-cubic equation of state for phase-equilibrium calculations. effect of density-dependent mixing rules," *Computers & chemical engineering*, vol. 12, no. 5, pp. 483–489, 1988.

[40] M. Castier, "Automatic implementation of thermodynamic models using computer algebra," *Computer & Chemical Engineering*, vol. 23, pp. 1229–1245, 1999.

[41] S. Dufal, T. Lafitte, A. Galindo, G. Jackson, and A. J. Haslam, "Developing intermolecular-potential models for use with the saft-vr m ie equation of state," *AIChE Journal*, vol. 61, no. 9, pp. 2891–2912, 2015.

[42] Z. Li, Z. Jin, and A. Firoozabadi, "Phase Behavior and Adsorption of Pure Substances and Mixtures and Characterization in Nanopore Structures by Density

Functional Theory," *SPE Journal*, vol. 19, no. 6, 2014.

[43] F. Dreisbach, R. Staudt, and J. U. Keller, "High pressure adsorption data of methane, nitrogen, carbon dioxide and their binary and ternary mixtures on activated carbon," *Adsorption*, vol. 5, no. 3, pp. 215–227, 1999.

[44] S. Qiao and X. Hu, "Using local IAST with micropore size distribution to predict desorption and displacement kinetics of mixed gases in activated carbon," *Separation and Purification Technology*, vol. 31, no. 1, pp. 19–30, 2003.

[45] S. H. Hyun and R. P. Danner, "Equilibrium adsorption of ethane, ethylene, isobutane, carbon dioxide, and their binary mixtures on 13x molecular sieves," *Journal of Chemical and Engineering Data*, vol. 27, no. 2, pp. 196–200, 1982.

APPENDIX A

DRA POTENTIAL RESULTS

This appendix contains tables presenting the binary and ternary mixture adsorption equilibria for mixtures of methane, nitrogen and carbon dioxide. The results are tabulated alongside the experimental data points reported by Dreisbach et al. [43]. Discussion of these results can be found in Section 4.2.

Table A.1: Binary adsorption equilibria of CH_4/N_2 mixtures on activated carbon at 298 K. P: bulk pressure (MPa); y_{CH_4} bulk composition of CH_4; N^{ads}: total amount of adsorbate (mol/kg); $x_{CH_4}^{ads}$: mole fraction of CH_4 in the adsorbate phase.

		Experimental Data		This Work	
P	y_{CH_4}	N^{ads}	$x_{CH_4}^{ads}$	N^{ads}	$x_{CH_4}^{ads}$
0.151	0.089	0.660	0.343	0.443	0.278
0.522	0.059	1.495	0.24	1.227	0.198
0.974	0.095	2.232	0.318	2.094	0.290
1.925	0.095	3.204	0.324	3.253	0.284
2.970	0.095	3.908	0.335	4.134	0.279
3.930	0.088	4.320	0.306	4.714	0.258
5.056	0.091	4.715	0.319	5.291	0.262
6.035	0.090	4.953	0.322	5.685	0.256
0.111	0.377	0.852	0.753	0.543	0.711
0.533	0.384	2.309	0.747	1.940	0.711
1.038	0.439	3.349	0.788	3.120	0.750
2.285	0.428	4.745	0.777	4.684	0.733
2.764	0.427	5.085	0.787	5.096	0.730
3.979	0.403	5.837	0.769	5.831	0.704
4.989	0.449	6.216	0.789	6.439	0.738
5.980	0.425	6.452	0.786	6.760	0.715
0.108	0.731	1.122	0.932	0.762	0.917
0.518	0.668	2.701	0.907	2.369	0.887
1.091	0.735	3.894	0.932	3.810	0.913
2.022	0.733	4.975	0.931	5.106	0.909
2.978	0.731	5.719	0.928	5.949	0.906
3.972	0.726	6.100	0.929	6.557	0.902
4.986	0.727	6.449	0.928	7.028	0.900
5.975	0.733	6.755	0.929	7.394	0.901

Table A.2: Binary adsorption equilibria of CH_4/N_2 mixtures on activated carbon at 298 K. P: bulk pressure (MPa); y_{CH_4} bulk composition of CH_4; Γ: surface excess of adsorbate (mol/kg); $x^{ex}_{CH_4}$: excess mole fraction of CH_4 in the adsorbate phase.

P	y_{CH_4}	Experimental Data		This Work	
		Γ	$x^{ex}_{CH_4}$	Γ	$x^{ex}_{CH_4}$
0.151	0.089	0.658	0.344	0.417	0.289
0.522	0.059	1.483	0.241	1.137	0.209
0.974	0.095	2.200	0.322	1.926	0.307
1.925	0.095	3.115	0.33	2.920	0.305
2.970	0.095	3.739	0.346	3.620	0.305
3.930	0.088	4.074	0.319	4.032	0.287
5.056	0.091	4.368	0.337	4.413	0.295
6.035	0.090	4.518	0.345	4.637	0.294
0.111	0.377	0.851	0.754	0.524	0.723
0.533	0.384	2.290	0.75	1.848	0.727
1.038	0.439	3.296	0.793	2.940	0.769
2.285	0.428	4.579	0.787	4.285	0.761
2.764	0.427	4.870	0.801	4.611	0.761
3.979	0.403	5.480	0.793	5.129	0.746
4.989	0.449	5.734	0.818	5.552	0.784
5.980	0.425	5.851	0.823	5.693	0.770
0.108	0.731	1.120	0.932	0.743	0.922
0.518	0.668	2.679	0.909	2.280	0.896
1.091	0.735	3.829	0.935	3.620	0.922
2.022	0.733	4.818	0.937	4.751	0.922
2.978	0.731	5.451	0.938	5.419	0.923
3.972	0.726	5.714	0.942	5.843	0.923
4.986	0.727	5.931	0.946	6.122	0.926
5.975	0.733	6.098	0.951	6.297	0.931

Table A.3: Binary adsorption equilibria of CH_4/CO_2 mixtures on activated carbon at 298 K. P: bulk pressure (MPa); y_{CH_4} bulk composition of CH_4; N^{ads}: total amount of adsorbate (mol/kg); $x^{ads}_{CH_4}$: mole fraction of CH_4 in the adsorbate phase.

| P | y_{CH_4} | Experimental Data | | This Work | |
		N^{ads}	x_{CH_4}	N^{ads}	x_{CH_4}
0.098	0.253	1.975	0.138	1.699	0.087
0.557	0.239	5.500	0.09	5.655	0.056
1.140	0.214	7.603	0.068	7.846	0.043
2.088	0.211	9.358	0.068	9.427	0.038
3.082	0.198	10.502	0.069	10.232	0.034
3.861	0.220	10.948	0.063	10.535	0.039
5.230	0.196	11.475	0.061	10.947	0.035
6.023	0.201	11.635	0.066	11.043	0.037
0.102	0.574	1.706	0.357	1.276	0.335
0.502	0.542	4.420	0.31	4.262	0.232
1.014	0.536	6.133	0.298	6.175	0.203
2.042	0.527	7.948	0.273	8.112	0.178
3.096	0.524	9.218	0.273	9.102	0.169
3.887	0.541	9.714	0.273	9.477	0.180
5.026	0.506	10.309	0.265	10.051	0.155
5.877	0.534	10.425	0.279	10.156	0.177
0.100	0.954	1.209	0.908	0.888	0.932
0.500	0.957	3.224	0.916	2.849	0.923
1.025	0.948	4.546	0.892	4.273	0.898
2.149	0.941	6.038	0.888	5.942	0.876
3.097	0.948	6.640	0.898	6.717	0.889
3.887	0.939	6.851	0.894	7.237	0.868
5.100	0.940	7.013	0.897	7.768	0.871
5.916	0.947	7.097	0.905	8.006	0.887

Table A.4: Binary adsorption equilibria of CH_4/CO_2 mixtures on activated carbon at 298 K. P: bulk pressure (MPa); y_{CH_4} bulk composition of CH_4; Γ: surface excess of adsorbate (mol/kg); $x_{CH_4}^{ex}$: excess mole fraction of CH_4 in the adsorbate phase.

P	y_{CH_4}	Experimental Data		This Work	
		Γ	$x_{CH_4}^{ex}$	Γ	$x_{CH_4}^{ex}$
0.098	0.253	1.972	0.138	1.682	0.085
0.557	0.239	5.456	0.089	5.557	0.053
1.140	0.214	7.475	0.066	7.641	0.038
2.088	0.211	9.058	0.064	9.036	0.031
3.082	0.198	9.976	0.062	9.623	0.024
3.861	0.220	10.233	0.052	9.740	0.024
5.230	0.196	10.352	0.046	9.754	0.015
6.023	0.201	10.236	0.048	9.575	0.012
0.102	0.574	1.704	0.357	1.259	0.332
0.502	0.542	4.387	0.308	4.174	0.225
1.014	0.536	6.041	0.294	5.996	0.193
2.042	0.527	7.702	0.264	7.739	0.161
3.096	0.524	8.769	0.260	8.516	0.144
3.887	0.541	9.107	0.255	8.723	0.149
5.026	0.506	9.432	0.243	9.026	0.115
5.877	0.534	9.367	0.250	8.922	0.128
0.100	0.954	1.207	0.908	0.871	0.931
0.500	0.957	3.199	0.916	2.763	0.922
1.025	0.948	4.474	0.892	4.093	0.896
2.149	0.941	5.833	0.886	5.558	0.872
3.097	0.948	6.300	0.893	6.156	0.884
3.887	0.939	6.417	0.891	6.522	0.861
5.100	0.940	6.417	0.893	6.808	0.861
5.916	0.947	6.386	0.900	6.878	0.877

Table A.5: Binary adsorption equilibria of CO_2/N_2 mixtures on activated carbon at 298 K. P: bulk pressure (MPa); y_{CO_2} bulk composition of CO_2; N^{ads}: total amount of adsorbate (mol/kg); $x_{CO_2}^{ads}$: mole fraction of CO_2 in the adsorbate phase.

		Experimental Data		This Work	
P	y_{CO_2}	N^{ads}	x_{CO_2}	N^{ads}	x_{CO_2}
0.108	0.189	0.964	0.758	0.585	0.6939
0.535	0.202	2.857	0.772	2.510	0.7820
1.058	0.216	4.119	0.774	4.103	0.8184
1.875	0.216	5.786	0.789	5.578	0.8310
3.078	0.217	6.452	0.799	6.904	0.8403
4.102	0.211	7.050	0.776	7.556	0.8368
5.066	0.180	7.411	0.761	7.670	0.7967
6.077	0.203	7.739	0.785	8.352	0.8281
0.109	0.489	1.530	0.915	1.244	0.9280
0.531	0.504	4.201	0.931	4.324	0.9524
1.048	0.488	5.661	0.936	6.134	0.9554
2.122	0.490	7.476	0.921	8.134	0.9612
3.061	0.487	8.344	0.927	9.033	0.9629
4.156	0.487	9.217	0.931	9.681	0.9640
5.015	0.480	9.904	0.933	9.989	0.9631
6.055	0.475	10.091	0.929	10.260	0.9620
0.116	0.794	2.206	0.978	1.940	0.9838
0.522	0.834	5.478	0.983	5.612	0.9914
1.000	0.883	7.278	0.989	7.730	0.9952
1.972	0.861	9.295	0.986	9.453	0.9949
2.901	0.895	10.403	0.99	10.326	0.9966
3.940	0.856	11.231	0.986	10.724	0.9951
5.023	0.874	11.633	0.988	11.036	0.9957
5.634	0.847	11.997	0.984	11.083	0.9944

Table A.6: Binary adsorption equilibria of CO_2/N_2 mixtures on activated carbon at 298 K. P: bulk pressure (MPa); y_{CO_2} bulk composition of CO_2; Γ: surface excess of adsorbate (mol/kg); $x^{ex}_{CO_2}$: excess mole fraction of CO_2 in the adsorbate phase.

P	y_{CO_2}	Experimental Data		This Work	
		Γ	$x^{ex}_{CO_2}$	Γ	$x^{ex}_{CO_2}$
0.108	0.189	0.962	0.759	0.566	0.7105
0.535	0.202	2.836	0.777	2.417	0.8042
1.058	0.216	4.057	0.783	3.919	0.8467
1.875	0.216	5.622	0.806	5.251	0.8694
3.078	0.217	6.169	0.825	6.362	0.8935
4.102	0.211	6.634	0.811	6.829	0.9035
5.066	0.180	6.871	0.807	6.771	0.8786
6.077	0.203	7.055	0.841	7.263	0.9219
0.109	0.489	1.528	0.916	1.225	0.9348
0.531	0.504	4.170	0.934	4.232	0.9623
1.048	0.488	5.576	0.943	5.951	0.9699
2.122	0.490	7.254	0.934	7.754	0.9843
3.061	0.487	7.976	0.948	8.475	0.9942
4.156	0.487	8.647	0.96	8.906	1.0056
5.015	0.480	9.137	0.971	9.039	1.0139
6.055	0.475	9.128	0.977	9.090	1.0247
0.116	0.794	2.203	0.978	1.920	0.9857
0.522	0.834	5.438	0.985	5.520	0.9940
1.000	0.883	7.172	0.991	7.551	0.9979
1.972	0.861	9.016	0.99	9.085	1.0004
2.901	0.895	9.917	0.995	9.756	1.0025
3.940	0.856	10.482	0.995	9.912	1.0065
5.023	0.874	10.554	0.999	9.913	1.0095
5.634	0.847	10.713	0.999	9.788	1.0139

Table A.7: Ternary mixture adsorption equilibria of $CH_4 - N_2 - CO_2$ mixtures on activated carbon at 298 K. P: bulk pressure in (MPa) ; y_{CH_4} and y_{CO_2}: mole fractions of CH_4 and CO_2, respectively, in the bulk phase; N^{ads}: total amount of adsorbate in (mol/kg); x_{CH_4} and x_{CO_2}: mole fractions of CH_4 and CO_2, respectively, in the adsorbate phase.

| P | y_{CH_4} | y_{CO_2} | Experimental Data | | | This Work | | |
			N^{ads}	x_{CH_4}	x_{CO_2}	N^{ads}	x_{CH_4}	x_{CO_2}
0.102	0.309	0.220	1.117	0.352	0.579	0.785	0.343	0.534
0.467	0.349	0.248	3.160	0.298	0.630	2.917	0.285	0.634
1.017	0.329	0.283	5.376	0.366	0.526	4.916	0.216	0.721
2.009	0.340	0.304	7.599	0.344	0.497	6.891	0.190	0.761
3.011	0.342	0.281	8.726	0.341	0.485	7.738	0.200	0.745
4.000	0.342	0.286	9.674	0.334	0.487	8.433	0.192	0.755
5.017	0.331	0.297	10.492	0.334	0.493	8.974	0.178	0.772
6.013	0.342	0.307	10.919	0.324	0.502	9.369	0.177	0.776
0.107	0.564	0.289	1.362	0.405	0.577	1.081	0.446	0.527
0.433	0.535	0.340	3.540	0.415	0.568	3.376	0.314	0.668
1.054	0.538	0.347	5.524	0.361	0.625	5.609	0.275	0.710
1.996	0.535	0.359	7.254	0.329	0.641	7.386	0.245	0.743
3.020	0.524	0.373	8.601	0.339	0.625	8.483	0.222	0.767
4.025	0.522	0.377	9.518	0.346	0.615	9.114	0.215	0.774
5.034	0.518	0.382	10.346	0.366	0.591	9.545	0.211	0.779
5.861	0.522	0.377	10.770	0.372	0.584	9.756	0.217	0.773
0.113	0.445	0.051	0.924	0.553	0.232	0.663	0.694	0.117
0.525	0.474	0.070	2.668	0.563	0.227	2.365	0.657	0.188
1.111	0.486	0.073	3.914	0.527	0.247	3.787	0.643	0.209
1.986	0.484	0.078	5.117	0.526	0.247	5.098	0.620	0.234
3.011	0.485	0.082	6.011	0.521	0.240	6.089	0.605	0.252
4.011	0.486	0.084	6.654	0.517	0.226	6.752	0.597	0.261
4.964	0.485	0.085	7.215	0.535	0.218	7.216	0.592	0.264
5.798	0.487	0.087	7.532	0.548	0.205	7.553	0.588	0.269

Table A.8: Ternary mixture adsorption equilibria of $CH_4 - N_2 - CO_2$ mixtures on activated carbon at 298 K. P: bulk pressure in (MPa); y_{CH_4} and y_{CO_2}: mole fractions of CH_4 and CO_2, respectively, in the bulk phase; Γ: surface excess amount of adsorbate in (mol/kg); $x^{ex}_{CH_4}$ and $x^{ex}_{CO_2}$: surface excess mole fractions of CH_4 and CO_2, respectively, in the adsorbate phase.

P	y_{CH_4}	y_{CO_2}	Experimental Data			This Work		
			Γ	$x^{ex}_{CH_4}$	$x^{ex}_{CO_2}$	Γ	$x^{ex}_{CH_4}$	$x^{ex}_{CO_2}$
0.102	0.309	0.220	1.116	0.352	0.579	0.767	0.343	0.541
0.467	0.349	0.248	3.139	0.297	0.632	2.836	0.284	0.645
1.017	0.329	0.283	5.296	0.366	0.530	4.738	0.212	0.738
2.009	0.340	0.304	7.373	0.344	0.503	6.534	0.182	0.786
3.011	0.342	0.281	8.337	0.341	0.495	7.195	0.189	0.780
4.000	0.342	0.286	9.127	0.334	0.499	7.698	0.178	0.800
5.017	0.331	0.297	9.740	0.334	0.508	8.036	0.160	0.827
6.013	0.342	0.307	9.968	0.322	0.520	8.220	0.154	0.842
0.107	0.564	0.289	1.360	0.404	0.577	1.062	0.444	0.531
0.433	0.535	0.340	3.517	0.414	0.569	3.301	0.309	0.675
1.054	0.538	0.347	5.439	0.359	0.629	5.424	0.266	0.723
1.996	0.535	0.359	7.036	0.323	0.650	7.027	0.230	0.763
3.020	0.524	0.373	8.200	0.330	0.638	7.924	0.201	0.795
4.025	0.522	0.377	8.910	0.334	0.632	8.348	0.187	0.811
5.034	0.518	0.382	9.495	0.352	0.609	8.558	0.175	0.825
5.861	0.522	0.377	9.734	0.357	0.606	8.580	0.175	0.827
0.113	0.445	0.051	0.923	0.553	0.232	0.643	0.702	0.119
0.525	0.474	0.070	2.648	0.563	0.228	2.274	0.664	0.192
1.111	0.486	0.073	3.849	0.528	0.250	3.594	0.652	0.216
1.986	0.484	0.078	4.965	0.528	0.252	4.749	0.630	0.246
3.011	0.485	0.082	5.738	0.523	0.248	5.555	0.616	0.269
4.011	0.486	0.084	6.249	0.519	0.235	6.033	0.610	0.282
4.964	0.485	0.085	6.665	0.540	0.229	6.317	0.607	0.290
5.798	0.487	0.087	6.859	0.554	0.216	6.494	0.605	0.299

Table A.9: Adsorption equilibria for binary mixtures of isobutane and ethylene on molecular sieve at three different temperatures and at a bulk pressure of 0.1378 MPa. $y_{iC_4H_{10}}$ is the mole fraction of isobutane in the bulk phase, N^{ads} is the absolute adsorbed amount of the mixture (mol/kg) and $x^{ads}_{iC_4H_{10}}$ is the mole fraction of isobutane in the adsorbate phase.

Bulk Phase	Experimental Data		This Work	
$y_{iC_4H_{10}}$	N^{ads}	$x^{ads}_{iC_4H_{10}}$	N^{ads}	$x^{ads}_{iC_4H_{10}}$
T = 298.15 K				
0.045	2.680	0.122	2.733	0.095
0.117	2.630	0.209	2.598	0.205
0.152	2.460	0.309	2.555	0.249
0.216	2.390	0.424	2.465	0.317
0.325	2.300	0.516	2.352	0.417
0.349	2.270	0.538	2.342	0.440
0.531	2.190	0.690	2.170	0.586
0.730	2.140	0.727	2.016	0.748
0.805	2.070	0.766	1.955	0.811
0.875	2.050	0.822	1.897	0.875
T = 323.15 K				
0.078	2.370	0.186	2.384	0.153
0.284	2.130	0.458	2.165	0.418
0.324	2.000	0.486	2.139	0.458
0.568	1.900	0.641	1.968	0.666
0.653	1.920	0.712	1.909	0.733
0.722	1.930	0.732	1.877	0.787
0.857	1.870	0.796	1.793	0.889
0.949	1.670	0.918	1.739	0.959
T = 373.15 K				
0.034	1.740	0.102	1.774	0.057
0.188	1.680	0.423	1.733	0.302
0.443	1.570	0.662	1.655	0.599
0.728	1.470	0.764	1.572	0.830
0.884	1.400	0.896	1.529	0.931
0.962	1.380	0.983	1.514	0.978

Table A.10: Adsorption equilibria for binary mixtures of isobutane and ethane on molecular sieve at two different temperatures and at a bulk pressure of 0.1378 MPa. $y_{iC_4H_{10}}$ is the mole fraction of isobutane in the bulk phase, N^{ads} is the absolute adsorbed amount of the mixture (mol/kg) and $x^{ads}_{iC_4H_{10}}$ is the mole fraction of isobutane in the adsorbate phase.

Bulk Phase	Experimental Data		This Work	
$y_{iC_4H_{10}}$	N^{ads}	$x^{ads}_{iC_4H_{10}}$	N^{ads}	$x^{ads}_{iC_4H_{10}}$
T = 298.15 K				
0.003	2.260	0.083	2.109	0.014
0.027	2.180	0.219	2.037	0.126
0.100	2.050	0.451	1.877	0.443
0.127	1.960	0.654	1.852	0.535
0.230	1.950	0.790	1.803	0.743
0.318	1.960	0.849	1.796	0.825
0.487	1.930	0.865	1.798	0.894
0.522	1.930	0.895	1.807	0.907
0.920	1.910	0.979	1.793	0.990
0.963	1.910	0.998	1.805	0.995
T = 323.15 K				
0.035	1.840	0.363	1.666	0.173
0.037	1.830	0.277	1.664	0.183
0.122	1.750	0.635	1.626	0.527
0.211	1.680	0.802	1.640	0.718
0.653	1.670	0.922	1.703	0.948
0.819	1.680	0.974	1.711	0.977
0.891	1.670	0.995	1.710	0.987

Table A.11: Adsorption equilibria for binary mixtures of ethylene and carbon dioxide on molecular sieve at two different temperatures and at a bulk pressure of 0.1378 MPa. $y_{C_2H_4}$ is the mole fraction of ethylene in the bulk phase, N^{ads} is the absolute adsorbed amount of the mixture (mol/kg) and $x^{ads}_{C_2H_4}$ is the mole fraction of ethylene in the adsorbate phase.

Bulk Phase	Experimental Data		This Work	
$y_{C_2H_4}$	N^{ads}	$x^{ads}_{C_2H_4}$	N^{ads}	$x^{ads}_{C_2H_4}$
T = 298.15 K				
0.066	3.980	0.075	3.758	0.024
0.090	3.930	0.090	3.742	0.033
0.293	3.780	0.190	3.585	0.138
0.493	3.650	0.296	3.397	0.294
0.697	3.350	0.482	3.170	0.524
0.889	3.070	0.728	2.939	0.813
T = 323.15 K				
0.094	3.410	0.087	3.213	0.046
0.304	3.290	0.266	3.060	0.179
0.602	3.000	0.474	2.811	0.460
0.682	2.880	0.580	2.740	0.557
0.900	2.660	0.834	2.550	0.854